Journal of The
Electrochemical Society

Protocol for the Ex-Situ Electrochemical Performance Evaluation of the High-Temperature PEMFC Electrodes: Activity, Durability and Wettability Inter-Relations

To cite this article: Rajan Maurya *et al* 2026 *J. Electrochem. Soc.* **173** 114507

Journal of The Electrochemical Society, 2026 **173** 114507

Protocol for the Ex-Situ Electrochemical Performance Evaluation of the High-Temperature PEMFC Electrodes: Activity, Durability and Wettability Inter-Relations

Rajan Maurya,[1] Per Morgen,[1] Saso Gyergyek,[2] Vahid Karimi,[1] Mengfan Zhou,[3] Na Li,[3] Fan Zhou,[3] Vincenzo Liso,[3] Raghunandan Sharma,[1,z] and Shuang Ma Andersen[1,z]

[1]*Department of Green Technology, University of Southern Denmark, Odense M, DK-5230, Denmark*
[2]*Department for Materials Synthesis, Jozef Stefan Institute, Ljubljana 1000, Slovenia*
[3]*AAU Energy, Aalborg University, Pontoppidanstræde 111, Aalborg, 9220, Denmark*

The effect of pre-wetting on the catalyst utilization and durability of high-temperature proton exchange membrane fuel cell (HT-PEMFC) gas diffusion electrodes (GDEs) was investigated in a three-electrode configuration. Pre-wetting protocols included treatment in ethanol-water mixture (0, 10, 50, and 100% v/v ethanol), ethanol-water vapor, and concentrated orthophosphoric acid (14.85 M) at 150 °C. All pre-wetting approaches significantly enhanced electrode wettability by reducing hydrophobicity and surface tension, thereby improving initial catalyst utilization. However, accelerated stress test (AST) revealed a trade-off between utilization and durability, with wetted electrodes exhibiting lower electrochemically active surface area and Pt retention than untreated electrodes. Changes in Pt crystallite and particle sizes during the AST were estimated through X-ray diffraction analysis and transmission electron microscopy. All three wetting procedures have similar effects on catalyst utilization and durability without compromising the structural integrity. Single-cell measurements showed that while pre-wetting is effective for rapid screening and improving the initial performance, its benefits are not directly transferable to practical operation without further optimization. These findings highlight the trade-off between catalyst utilization and durability in HT-PEMFC GDEs.
 [DOI: 10.1149/1945-7111/ae747a]

Manuscript submitted January 13, 2026; revised manuscript received May 27, 2026. Published June 10, 2026.

Supplementary material for this article is available online

Development of electrocatalysts and electrodes with optimal interface is of utmost importance for efficient electrochemical devices, including fuel cells and electrolyzers, promising devices for green and sustainable energy conversion. This development requires an efficient and inexpensive electrocatalyst for oxygen reduction reaction, oxygen evolution reaction, and hydrogen evolution reaction. Electrocatalytic activity of these catalysts is generally assessed through a rotating disk electrode (RDE) configuration or membrane electrode assembly (MEA).[1,2] The simple RDE set-up provides a quick first check on the intrinsic catalytic activity. RDE technique with aqueous electrolytes is employed for the initial screening of catalysts in the early stages of catalyst development, when catalysts are available in minute quantities. In the RDE technique, a few milligrams of catalyst are drop-coated or deposited on a conductive substrate (such as carbon or gold) embedded in the RDE rotator.[3] The hydrodynamic condition establishes a well-defined diffusion layer, which allows the extraction of important kinetic parameters (exchange current density, Tafel slope, mass/area specific activity) of the reactions on the catalyst surfaces.[4] On the other hand, although complex, the MEA configuration testing resembles the actual operational conditions. The five-layer MEA is constructed by sandwiching the membrane with two gas diffusion electrodes (GDEs), which are finally sealed between two flow fields to form a single-cell unit. However, construction of such MEA is time-consuming and requires capital-intensive complex instruments to control gas pressure, temperature, humidity, etc.

The fundamental differences in the testing conditions of these two setups (RDE and MEA) arise from various factors, including the different catalyst ink compositions (ionomer/catalyst ratio), catalyst loading, and substrate on which the ink is coated (its conductivity, porosity, roughness, etc.). Moreover, the thickness of the catalyst layer (CL) in MEA and RDE differs significantly: the former is a few micrometers thick, while the latter is a few nanometers thick. This difference in CL thickness has a huge impact on the transport properties of the reacting species and products within the CL.[5,6] In MEA, the reacting gases can reach the thick CL (reaction site) via gas diffusion through the flow field and the gas diffusion layer (GDL), ultimately crossing the thin ionomer. In the RDE setup, although the CL is much thinner (a few nanometers), the pores are flooded with the liquid electrolyte, increasing the diffusion length for reacting species (e.g., O_2 gas) to a few micrometers.[6]

To reduce the gap between RDE and MEA catalyst performance evaluations, several methods/techniques that enable high mass-transport in liquid electrolytes have been proposed/developed. These methods include the floating electrode technique, half-MEAs, microelectrodes, and testing of individual GDEs in three-electrode configuration, etc.[7–10]

Based on the difference in the operation temperature, fuel cells are categorized into 1) low-temperature PEMFC (LT-PEMFC) and 2) high-temperature PEMFCs (HT-PEMFC). The operational temperature of LT-PEMFC is within 100 °C, and it has the advantages of fast start-up and higher performance.[11,12] These advantages are partially due to the use of proton conductive perfluorosulfonic acid (PFSA) based membranes such as Nafion. However, the conductivity of such membranes depends on the water content, which requires complex water and thermal management to avoid membrane dehydration or flooding of electrodes. Also, LT-PEMFCs are more susceptible to CO poisoning, which is present in trace amounts in the feed H_2 gas.[13] The HT-PEMFCs operate in the temperature range of 100 °C–200 °C, which have the following advantages: 1) improved reaction kinetics, 2) simple water management because the product is in gaseous state,[14,15] and 3) high CO tolerance (~3%).[16] Generally, polybenzimidazole (PBI)-based membranes and polytetrafluoroethylene (PTFE)-based binders are used in the electrode CL of HT-PEMFCs. Commonly used PTFE ionomer content in the CL is high (approximately 30 wt% of the catalyst), and it is highly hydrophobic in nature. However, HT-PEMFCs suffer from slow start-up, relatively lower performance, high Pt loading requirement, and comparatively shorter lifetime.[17]

Although high operating temperature solves water management issues in HT-PEMFCs, the overall cell performance is influenced by the catalyst utilization, which is directly related to the hydrophobicity and wettability of electrodes. To enhance the catalyst utilization

[z]E-mail: rash@igt.sdu.dk; mashu@igt.sdu.dk

and electrode wettability, various strategies such as 1) variation of PTFE content in the CL,[18] 2) use of surfactants in the coating process for better dispersion,[19] 3) electrochemical potential cycling,[20,21] 4) thermal treatment of the electrodes at high temperature[22,23] etc., are reported in the literature.

In comparison to the LT-PEMFCs, HT-PEMFCs suffer from a longer activation time, which can be as long as 100 h.[24] During the break-in/activation procedure, the cell performance increases to the maximum and remains stable afterward. The cell activation procedures can be broadly classified into two categories: 1) online activation and 2) offline activation. In the offline method, all activation protocols for various cell components are applied before assembling the full cell therefore no electronic load or bench is required.[25] The offline break-in procedure includes MEA steaming/boiling, membrane plasma sputtering, GDL compression, etc.[26–29] In the online method, all the procedures are performed in situ that includes load profile activation, high temperature/pressure activation, pulsed activation, super saturated activation, air braking, reverse flow etc.[27,30–35] To reduce the cost related to the activation and lower the activation time, several approaches for the activation including application of high current density, voltage scanning, voltage stepping, cathode starving and short circuiting are proposed.[25,36] Tsotridis et al. have demonstrated a cathode starvation (stopping the oxygen supply while the cell is under the load) approach for faster activation.[30] These cell activation procedures are usually performed under fully humidified conditions (100% relative humidity at both anode and cathode), and they alter the porosity of the CL, catalyst shape and size, polymer chain orientation, etc., which ultimately impacts the durability of the cell.[25] In contrast to the carbon cloth-based GDLs, the carbon paper-based GDLs pose a variety of challenges in the initial cell break-in process. Carbon paper is relatively thin, more brittle, and less forgiving during the hydration and compression cycles that require a more delicate break-in/activation process, and careful control of pressure/humidity, with an increased risk of both flooding and drying out.[37]

Triple phase boundary (TPB) is a critical site where the reacting gas, liquid electrolyte, and solid catalyst meet, and the electrochemical reaction takes place.[38] Garcia et al. investigated the impact of catalyst and its support/GDL wettability at the TPB and its effect on proton transport in the ionomer using molecular dynamics simulations.[39] Their study suggests that the transport mechanism of reacting gas (oxygen), water, and protons is affected by the level of hydrophobicity at TPB, as poor water transport may lead to lower performance. Proper water transport at the TPB is essential for maintaining continuous proton and oxygen flow and for improving cluster interconnection.[40,41] Therefore, to enhance catalyst performance and utilization, it is crucial to improve the accessibility of the TPB. Consequently, enhancing TPB accessibility and wettability is vital for achieving better performance, higher catalyst utilization, and faster break-in. In the present work, HT-PEMFC GDEs were wetted under different conditions and the effect of wetting conditions on electrodemorphology, catalyst utilization, was investigated through scanning electron microscopy (SEM) imaging, theoretical physical surface area (PSA), and electrochemical active surface area (ECSA). The GDEs wetted in different conditions were subjected to an accelerated stress test (AST) in a three-electrode configuration liquid cell. The effects of different wetting conditions on durability, crystallinity, and catalyst retention were studied through X-ray diffraction (XRD), X-ray fluorescence (XRF), and transmission electron microscopy (TEM). Also, the impact of the ethanol wetting protocol on cell break-in/activation was investigated on the MEAs constructed with carbon paper and carbon cloth-based GDL.

Experimental

Materials.—Orthophosphoric acid (H_3PO_4, 98% with stated purity 98%, pH < 0.50) was procured from Merck. Absolute ethanol (100%) (from Merck) and ultra-pure water (resistivity ~18.2 MΩ-cm) obtained from Voela were used to prepare the ethanol water mixture. GDEs, namely GDE-1 and GDE-2, were prepared using a commercial Pt/C (Pt/C-01; ~60 wt% Pt on a high surface area carbon support, BET surface area 34.6 $m^2\ g^{-1}$ and particle size 5.5 nm) and a homemade Pt/C (Pt/C-02) with a similar Pt loading on a commercial high surface carbon (C350G, Imerys Carbon) support, respectively. The homemade Pt-based catalyst Pt/C-02 was synthesized on C350G (Imerys) carbon support with a particle size of 3.5 nm, 286 $m^2\ g^{-1}$ BET surface area, and 0.00810 $cm^3\ g^{-1}$ pore volume. A SIGRACET® 35 DC carbon paper-based GDL from SGL CARBON GmbH was used to prepare GDEs. The SIGRACET® 35 DC GDL used in this study is a non-woven carbon paper gas diffusion media with a microporous layer that has been PTFE treated to 5 wt%. It has a total thickness of 285 μm.

GDE preparation.—The GDEs were prepared by role-to-role printing (slot-die method) of a catalyst ink containing the Pt/C electrocatalyst and other ingredients, tailored for HT-PEMFC electrode applications, onto the GDL (area: 10 cm × 18 cm). The exact catalyst layer composition and ink composition, including the binders and ionomers, were similar to those described in earlier report.[42] The areal Pt loadings in the GDE-1 and GDE-2 were ~0.8 mg cm^{-2} and ~0.4 mg cm^{-2}, respectively, as determined by the XRF spectroscopy using a Niton XL3t GOLDD + handheld XRF analyzer (Thermo Scientific) instrument. A user-defined method (calibrated with a sample of a known amount of Pt) was employed to interpret the spectra and estimate the Pt loadings (mg cm^{-2}). Furthermore, for structural and electrochemical characterizations, GDE disk samples with a diameter of 10 mm were punched from the printed GDEs.

Electrochemical characterizations.—All the electrochemical measurements were conducted with a Biologic VMP 300 potentiostat (Biologic Instruments, Seyssinet-Pariset France) in a custom-made three-electrode configuration. A double junction Ag/AgCl (sat. KCl) and a graphite rod (diameter ~10 mm) were used as reference and counter electrode, respectively. GDE disk of 10 mm diameter was working electrode (WE).The WE was mounted on a customized sample holder utilizing a thin graphite rod (0.5 mm diameter) contact (Figure S1 in supporting information (SI)). To mimic the harsh operating conditions of HT-PEMFCs, a highly concentrated (14.85 M) H_3PO_4 was used as the supporting electrolyte for all electrochemical measurements. To remove dissolved oxygen, the supporting electrolyte was purged with high-purity argon for 10 min prior to any measurement, and purging was continued throughout the experiment. Prior to AST cycling, the electrode was activated by potential cycling (0.02 V–1.2 V) for 50 cycles (unless otherwise stated) at a scan rate of 0.05 V s^{-1}. The AST cycling was performed over the potential range of 0.4 V–1.6 V for 1600 cycles at a scan rate of 1 V s^{-1}. Intermittent observational/slow scan cyclic voltammograms (CVs) were recorded before, during, and after the AST in the potential range of 0.02 V–1.2 V at a scan rate of 0.01 V s^{-1}. All the electrochemical experiments were conducted at room temperature under stationary conditions. Active iR compensation was applied in all cyclic voltammetric analyses. The solution resistance estimated from the built-in impedance spectroscopy (at 10 kHz) was used for iR compensation in all measurements. The ECSA was calculated from the charge associated with cathodic hydrogen underpotential deposition (H_{upd}). A normalization factor (surface charge density) of Pt polycrystalline, i.e., 210 μC cm^{-2}, was used in ECSA calculations.[43] To ensure the statistical robustness and add the standard error bars, all the experiments were repeated three times.

Wetting procedure.—To study the effect of the wetting procedure on their electrochemical performance, the GDE-1 and GDE-2 samples were wetted using different wetting procedures, namely(1) the ethanol-water solution (EWS) wetting using ethanol/water ratios of 0/100, 10/90, 50/50 and 100/0 v/v respectively,(2) the ethanol-

water vapor (EWV) wetting using ethanol/water ratios of 0/100 or 50/50 v/v and (3) the high concentration acid (HCA) wetting at 150 °C, as summarized in Table I. All the wetting treatments were performed on the GDE working electrodes just before mounting them in the three-electrode setup for the electrochemical measurements.

Single-cell pre-wetting and break-in test.—To further investigate the effect of ethanol pre-wetting, this treatment was carried out in a single fuel cell. The single-cell hardware consists of a MEA based on carbon paper GDLs, featuring a rectangular active area of 165 cm^2 and platinum catalyst on both sides. Graphite composite flow plates with a serpentine channel pattern (1 mm wide, 1 mm deep, and 1 mm spacing) are employed on both the anode and cathode sides. Gas sealing between the MEA and the flow plates was achieved using PTFE gaskets with a thickness of 250 μm, and a compression force of 10.5 kN was applied to the assembly. The single cell was connected to a Greenlight fuel cell test station (Greenlight Innovation, Canada), which provides automated control of key operating parameters, including cell temperature, gas stoichiometry, relative humidity, back pressure, anode and cathode mass flow rates, and load switching.

The ethanol pre-treatment protocol applied in the single high-temperature PEM fuel cell test is illustrated in Fig. S2 in SI. The single cell was assembled, installed in a Greenlight test station, and subjected to a leak check using dry N_2 to ensure gas tightness. After verifying the mass flow controllers, all heated lines and the ethanol evaporator were activated. N_2 was introduced to the anode as a carrier gas at a flow rate of 1.0 l min^{-1}, while the evaporator and mixing section were heated to 100 °C to prevent ethanol condensation. Once thermal stability was achieved, liquid ethanol was fed into the evaporator at 1 ml min^{-1}, generating ethanol vapor that was mixed with the N_2 stream to obtain an ethanol content of 34% in the inlet mixture, as defined by the system's mixing calculation. In parallel, the cell temperature was increased and subsequently maintained at 120 °C. After stabilization, the ethanol–N_2 mixture was supplied to the anode, and the cell was operated under the predefined pre-treatment mode for 10 min, during which voltage, current, and inlet/outlet conditions were continuously recorded. Following pre-treatment, the ethanol feed was stopped, and the anode was purged with N_2 to remove residual ethanol vapor. A standard break-in procedure was then initiated, with H_2 supplied to the anode and air to the cathode at stoichiometries of 1.25 and 2.5, respectively. The cell was operated at a constant current density of 0.2 A cm^{-2} for 44 h to ensure full electrode activation, and the cell performance was monitored throughout the break-in and subsequent stabilization period.

Structural characterization.—The effect of ethanol and high-temperature wetting on the morphology and the integrity of electrodes was analyzed through SEM imaging using a FEI Quanta 200 SEM operated at 20 kV. Further, a JEOL JEM-2100 transmission electron microscope (TEM) operated at 200 kV was used to acquire TEM images of selected samples, which were analyzed to obtain the pre-AST and post-AST particle size distributions of the Pt nanoparticles in the CLs. For TEM sample preparation, the GDE was transferred to a 25 ml sample collection bottle containing 20 ml of pure ethanol. The bottle was then ultrasonicated in a room-temperature water bath for 15 min to detach the catalyst layer into the ethanol, resulting in a suspension of catalyst particles. This suspension was used for TEM characterization. Finally, XRD patterns of the pre-AST and post-AST GDEs were acquired using a Rigaku Miniflex 600 X-ray diffractometer equipped with a Cu Kα ($\lambda = 1.5418$ Å) radiation source. The XRD patterns were recorded over a 2θ range of $10° - 90°$ at a scan rate of 5° min^{-1} with a step size of 0.02°. The full width at half-maximum (FWHM) of the Pt (111) peak at ~40° was obtained by fitting the corresponding spectra with a Lorentzian distribution using the software XPSpeak4.1.

Results and Discussion

Demonstration of the wettability issue through cyclic voltammetry.—The observational CVs recorded on the GDE-1 and GDE-2 electrode samples (EWS-00 wetting; standard activation; Ar-saturated 14.85 M H_3PO_4; scan rate: 0.01 V s^{-1}; Figs. 1a, 1b may be compared with the corresponding CVs recorded on thin-film

Table I. Summary of different GDE wetting procedures explored.

Wetting procedure	Description				
Ethanol-water solution (EWS) wetting	**Objective:** To wet the GDE surface by lowering the surface tension of the solvent.				
	Procedure: (i) Dipping the GDE in aethanol-water mixture followed by visual inspection of air bubbles on the GDE (after pulling out of the liquid); (ii) Repeating step (i) till the GDE surface (catalyst layer side) appears free from air bubbles; (iii) Cleaning the GDE by dipping in ultrapure water (~20 ml) for 15 s and repeating the step with a different water reservoir to ensure complete removal of ethanol; (iv) transferring the wetted electrode sample to the three-electrode setup for the measurements				
	Wetting temperature	25 °C			
	Ethanol/water ratio (v/v)	0/100	10/90	50/50	100/0
	Sample ID	EWS-00	EWS-10	EWS-50	EWS-100
Ethanol-water vapor (EWV) wetting	**Objective:** To investigate an alternative route to EWS wetting, which could potentially be used as a wetting procedure during single-cell testing				
	Procedure: (i) Holding the GDE for 10 min in an ethanol-water vapors generated by boiling a water-ethanol mixture (ethanol/water ratio of 50/50 v/v) or water; (ii) transferring the wetted electrode sample to the three-electrode setup for the measurements				
	Wetting temperature	100 °C			
	Ethanol/water ratio in mixture (v/v)	0/100		50/50	
	Sample ID	EWV-00		EWV-50	
High-concentration acid (HCA) wetting	**Objective:** To wet the GDE by exposing it to harsh conditions similar to those for the HT-PEMFC operation				
	Procedure: 1. (i) Dipping the GDE in 14.85 M H_3PO_4 (heated to 150 °C); (ii) ensuring the GDE surface is free from air-bubbles by gentle agitation; (iii) holding the GDE in the heated acid for 10 min; (iv) transferring the wetted electrode sample to the three-electrode setup for the measurements				
	Wetting temperature	150 °C			
	Sample ID	HCA-150			

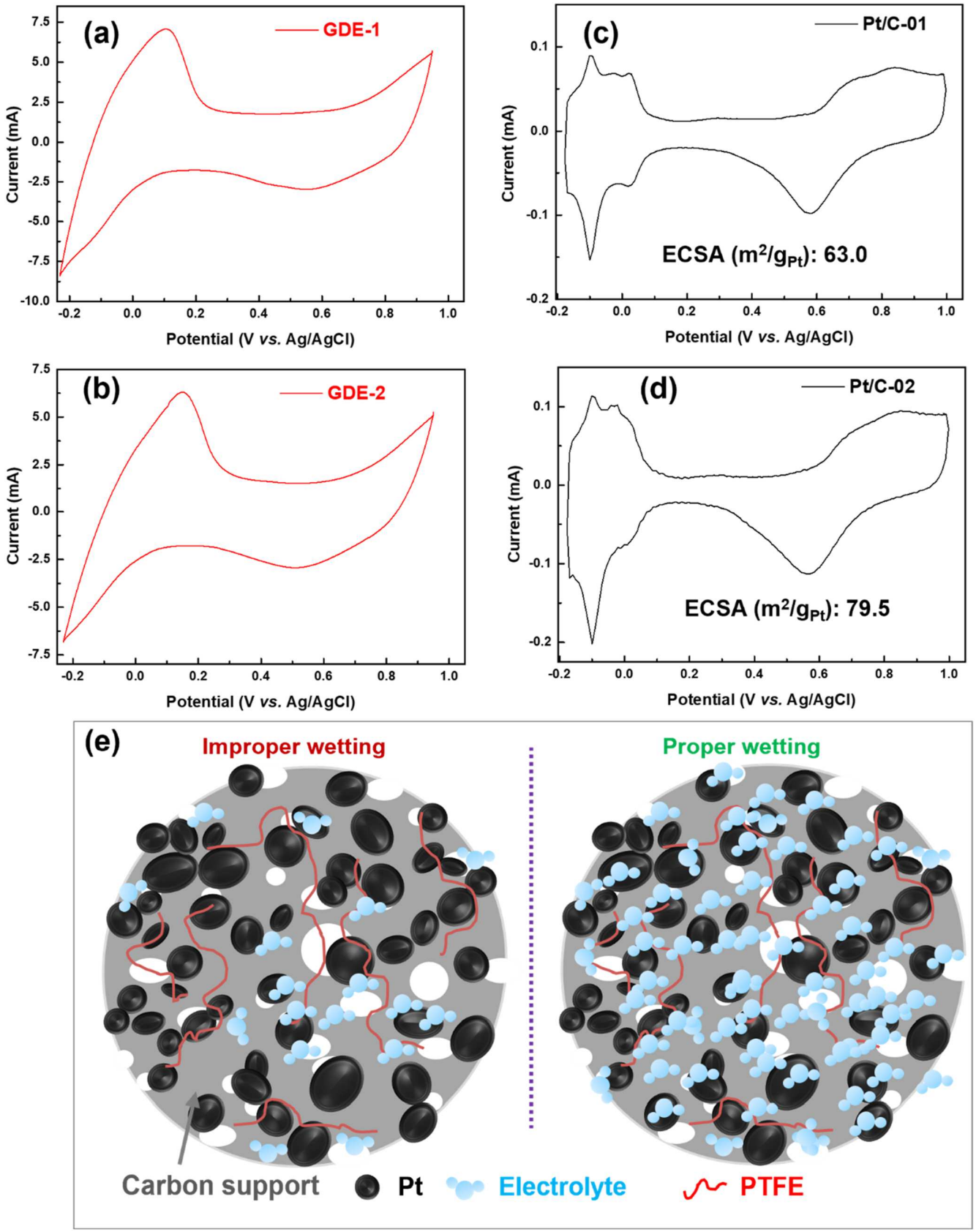

Figure 1. Cyclic voltammograms recorded on the (a) GDE-1 electrode and (b) GDE-2 electrode (wetting procedure EWS-00), in Ar-saturated 14.85 M H_3PO_4 at a scan rate of 0.1 V s^{-1} and on the GC electrodes modified with the thin-film catalyst layers of (c) Pt/C-01 and (d) Pt/C-02 electrocatalysts in Ar-saturated 1.0 M H_3PO_4; scan rate: 0.01 V s^{-1}. (e) schematic showing different constituents of the catalyst layer in the HT-PEMFC GDEs with improper (left) and proper (right) wetting by the electrolyte.

catalyst layer modified glassy carbon (GC) electrodes (Figs. 1c, 1d) using Pt/C-01 and Pt/C-02 catalysts, respectively. The CVs in GC-RDE configuration was recorded in argon-saturated 1.0 M H_3PO_4 at a scan rate of 0.01 V s^{-1};. For the thin-film CL modified GC electrode studies, standard catalyst ink consisting of the Pt/C electrocatalyst and Nafion ionomer in 70/30 w/w ratio were drop casted on a cleaned GC disc electrode (diameter: 5 mm) and spin dried at room temperature (for details, see Ref. 44).

In contrast to the case for the voltammograms corresponding to the GC electrodes, the hydrogen underpotential deposition (H_{upd}) on Pt and the Pt oxide formation/reduction features are not clear in those corresponding to the GDE-1 and GDE-2 electrodes, despite their reasonably high Pt loading values. This partial/distorted Pt feature indicates that the GDE is initially hydrophobic, and all the Pt sites are not exposed to the electrolyte. Also, due to the presence of a PTFE binder in the thick CL of GDE, the initially distorted Pt features in the CVs arise from high hydrophobicity, contact resistance, and in-plane resistance to electrolyte transport. The initial ECSA values for the GDE-1 and GDE-2 electrodes are estimated to be ~34 m^2 g^{-1}_{Pt} and 43 m^2 g^{-1}_{Pt}, respectively. These ECSA values are significantly lower than those obtained for the Pt/C-01 and Pt/C-02 electrocatalysts from the GC electrode measurements (Figs. 1c, 1d). This noteworthy difference between the voltammograms for the GDEs and the GC electrodes may be attributed to the improper wetting of the HT-PEMFCs GDEs by the electrolyte due to the presence of hydrophobic polymeric binders such as PTFE in the CL (Fig. 1e), hindering the electrolyte accessibility to the catalytically active sites during room-temperature half-cell studies. To further demonstrate the improper wetting under EWS-00 conditions, a 100-cycle activation followed by 5100 AST cycles was performed. As expected, the features of the cyclic voltammograms remain unchanged after the 100 activation cycles (Fig. S3a in SI). Additionally, ECSA remains nearly constant at ~32 m^2 g^{-1}_{pt} even after 5100 AST cycles (Fig. S3b, c in SI). These observations further confirm the improper wetting under EWS-00 conditions. Therefore, for proper wetting of the CL in the HT-PEMFC GDEs, exploration of a suitable wetting procedure is essential to overcome the limitations of the simple water wetting (EWS-00) procedure.

Protocol development for half-cell electrochemical characterization of the HT-PEMFC GDEs.—Here, different surface wetting treatments are explored to reduce the hydrophobicity of the GDEs and thereby improve electrolyte accessibility to the GDE surface. Essentially, the wetting treatments studied here can be classified into two categories, i.e., (i) using a low surface tension liquid to wet the GDE surface or (ii) lowering the hydrophobicity of the GDE surface temporarily by changing the surface functionality. As an example of the former approach, the GDE surface may be wetted by a low surface tension solvent miscible with water and/or aqueous electrolyte e.g., ethanol-water mixture. For the GDEs to be studied in

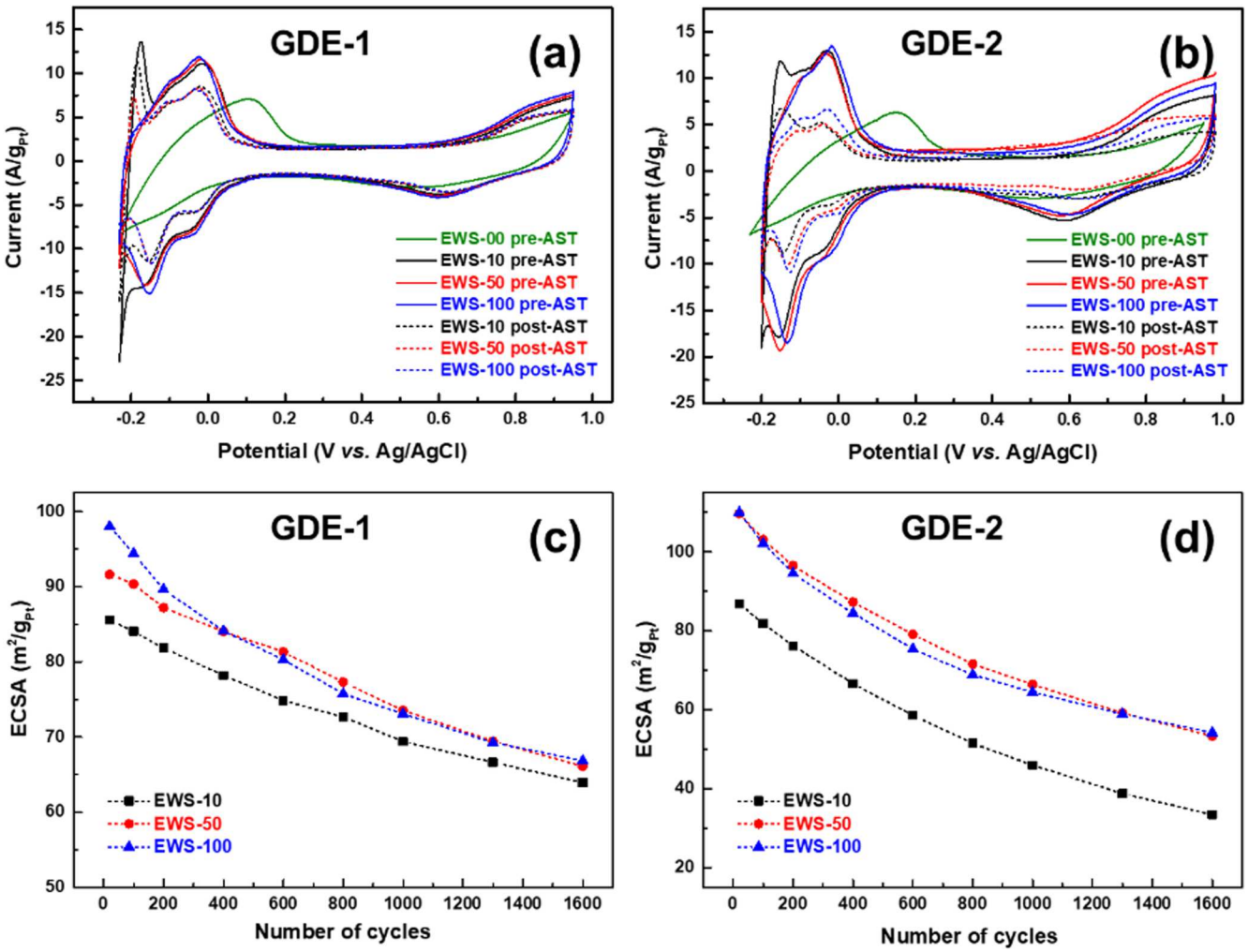

Figure 2. Cyclic voltammograms corresponding to the GDEs subjected to EWS wetting for different ethanol/water volumetric ratios of 0/100 (EWS-00), 10/90 (EWS-10), 50/50 (EWS-50), and 100/0 (EWS-100) from (a) GDE-1 electrode and (b) GDE-2 electrode. The voltammograms are recorded in Ar-saturated 14.85 M H_3PO_4 at a scan rate of 0.01 V s^{-1}. The solid and dashed lines represent the pre-AST and post-AST CVs, respectively, while no AST was performed on EWS-00 electrodes due to the absence of Pt features in the voltammogram. Variations in ECSA with the number of potential cycles during the AST for the EWS-wetted GDEs from (c) GDE-1 and (d) GDE-2.

aqueous electrolytes, the solvent is subsequently displaced by water/aqueous electrolyte after wetting, allowing electrolyte accessibility to the electrocatalytic sites. As another example, the surface tension of the electrolyte can be reduced by increasing the temperature, thereby improving the GDE surface wettability. Similarly, adsorption of polar molecules on the GDE surface, for example by exposing it to solvent (e.g., water/ethanol-water) vapors, can be used to reduce its hydrophobicity. The wetting procedure can be explained as follows: Wettability describes how well a liquid interacts and spreads on a solid surface. It is governed by the balance between adhesive forces (attraction between the liquid and the solid) and cohesive forces (attraction between liquid molecules). When cohesive forces are stronger, liquid spreads over the surface, indicating high wettability. In contrast, when cohesive forces dominate, the liquid forms droplets, resulting in low wettability. Due to the use of PTFE, the GDE surface is highly hydrophobic. Simply dipping the GDE in water or electrolyte, the cohesive forces dominate, resulting in lower wettability. Mixing water with ethanol weakens cohesion and lowers surface tension. This lower tension allows the liquid to enter, fill, and permeate the CLs surface texture and pores. Once the pores are wetted by the ethanol-water mixture, the electrolyte is also readily accessible to Pt nanoparticles in the CL. Systematic experiments exploring the impacts of such treatments on the GDE surface wettability are presented here.

Ethanol-water solution (EWS) wetting.—As described in Table I, EWS wetting treatments were performed using four different EWS compositions with varying ethanol volume fractions of 0%, 10%, 50% or 100%. Figures 2a, 2b shows the CVs recorded on the GDE-1 and GDE-2 electrodes, initially wetted in 0% (EWS-00), 10% (EWS-10), 50% (EWS-50), and 100% (EWS-100) ethanol-water solution, in Ar-saturated 14.85 M H_3PO_4. Typical Pt polycrystalline features in acidic conditions, i.e., 1) H_{upd} (0.02 V–0.350 V), 2) double layer charging (0.350 V–0.550 V), and 3) oxide formation (0.550 V–1 V), were observed in the voltammograms. The initial ECSA (prior to AST) was influenced by the ethanol volume fraction used in the wetting process. With an increase in the ethanol fraction (from 0% to 50%) in the EWS, the initial ECSA increased, indicating that more Pt catalyst sites are in contact/exposed to the electrolyte due to improved wetting, as explained earlier. Further, the initial ECSA values for the EWS-50 and EWS-100 samples were comparable, suggesting complete wetting for the EWS-50, hence saturation of the ECSA value for the ethanol fractions >50%. Both electrodes (GDE-1 and GDE-2) show similar trends, indicating that wettability is independent of the Pt nanoparticles size and the carbon support type.

Further, the area/charge values in the H_{upd} region and oxide formation region of the voltammogram decrease (Figs. 2a, 2b dashed lines) for the post-AST cyclic voltammograms (electrodes subjected to AST), indicating activity degradation of the Pt/C electrocatalyst. Figure 2c, 2d shows that the ECSA of both the electrodes decreases with the number of potential cycles during the AST. However, the decreasing trend and final ECSA value depend on the ethanol fraction used to wet the electrode. The electrodes wetted in 50% and 100% ethanol solutions show similar trends. On the other hand, the electrodes wetted in 10% ethanol showed lower ECSA loss during the AST assessment than those wetted in 50% or 100% ethanol-water solutions. During the potentiodynamic AST of GDEs in liquid electrolytes, different degradation mechanisms, including (i) the growth of the Pt nanoparticles (Ostwald ripening) through dissolution and redeposition of Pt, (ii) the degradation of PTFE binder/ionomer in the CL, and (iii) the loss of Pt loading through dissolution, are widely reported in the literature.[10,38] Here, the Pt loss/retention during the AST assessment was calculated from the Pt loading (mg cm^{-2}) obtained from the XRF measurements of pre-AST and post-AST electrodes. The Pt retained in the post-AST GDE-1 electrode, and GDE-2 electrode wetted in different ethanol fractions are summarized in Table II. As the ethanol fraction used to wet the electrodes increases, Pt retention decreases. This trend in Pt retention with ethanol fraction correlates well with that of ECSA retention, which also decreases with increasing ethanol fraction used to wet the electrodes. This is further discussed in terms of the effects of EWS wetting on the catalyst utilization factor, the growth rate of Pt crystallites, and Pt dissolution during the AST.

Table II. Pt crystallite size values obtained from the XRD patterns of pre-AST and post-AST GDE samples wetted in EWS-00, EWS-10, EWS-50, EWS-100 solutions.

Sample	Ethanol fraction (vol%)	Crystallite size (nm)	
		Pre-AST	Post-AST
GDE-1 electrode	10 (EWS-10)	5.5	6.0
	50 (EWS-50)	5.5	6.2
	100 (EWS-100)	5.5	6.3
GDE-2 electrode	10 (EWS-10)	3.5	6.5
	50 (EWS-50)	3.5	7.6
	100 (EWS-100)	3.5	7.4

Effect of EWS wetting on crystallite size, utilization and retention of Pt.—XRD patterns recorded on the pre-AST and post-AST GDE-1 electrode (Fig. 3a) and GDE-2 electrode (Fig. 3b) samples wetted through EWS wetting procedure exhibit diffraction peaks centered at 2θ values of ~18°, ~26°, and ~40°, which correspond respectively to the binder PTFE,(100) graphitic carbon(002), and Pt.(111) Other prominent diffraction peaks at 2θ values of ~46°, ~68°, ~82°, and ~86° correspond to the Pt,(200) Pt,(220) Pt,(311) and Pt(222) diffractions, respectively. In pre-AST electrodes, the Pt(111) peak appears relatively broad for all the studied GDEs and becomes sharp after the electrodes were subjected to AST cycling (Figs. 3a, 3b), indicating significant changes in the Pt crystallite size (L) during the AST. The average crystallite size (L) of Pt(111) was calculated by the Scherrer Eq. E1.[44,45]

$$L = (0.94 \times \lambda)/(\beta \times \mathrm{Cos}\theta) \qquad [E1]$$

Here, λ (1.5418 Å) is the wavelength of X-rays; β is the FWHM ($\Delta 2\theta$) of the Pt)(111) diffraction peak centered at $2\theta \sim 40°$. For the Scherrer analysis, the instrumental broadening was considered negligible as the associated error was estimated to be within 1%. (Figure S4 and Table ST1 in SI). As summarized in Table II, the average Pt crystallite sizes of the electrodes wetted in various ethanol fractions increase during AST, with a higher increment for those wetted using higher ethanol fractions. This is due to reduced hydrophobicity, which exposes more Pt sites to the electrolyte, increasing the number of sites available for dissolution and redeposition. Due to the lower PTFE content in the CL, the GDE-2 electrode showed a relatively higher increase in the crystallite size. The trend in Pt crystallite size in post-AST electrodes is in line with the ECSA loss trends observed in electrodes wetted in different ethanol fractions.

The effect of EWS wetting was also investigated by TEM imaging. Prior to the EWS wetting, Pt/C catalysts show uniform distribution of Pt nanoparticles on both the GDE-1 and GDE-2 samples (Fig. 3c, 3d). The Pt particle size in fresh GDE-1 and GDE-2 electrodes is ~2.4 nm and ~2.6 nm, respectively (inset of Fig. 3c, 3d). As expected, EWS wetting has a significant impact on the Pt particle size and distribution in the post-AST GDEs, with the post-AST average Pt particle sizes for the GDE-1 and GDE-2 electrodes being observed to be ~3.6 nm and ~4.5 nm, respectively. The trends in the post-AST Pt crystallite sizes, estimated from XRD patterns and TEM imaging, agree well with each other.

The average Pt crystallite size of the pre-AST electrode, determined from the Scherrer equation, was used to calculate the theoretical physical surface area (PSA) of Pt in the corresponding Pt/C electrocatalyst (Eq. E2).

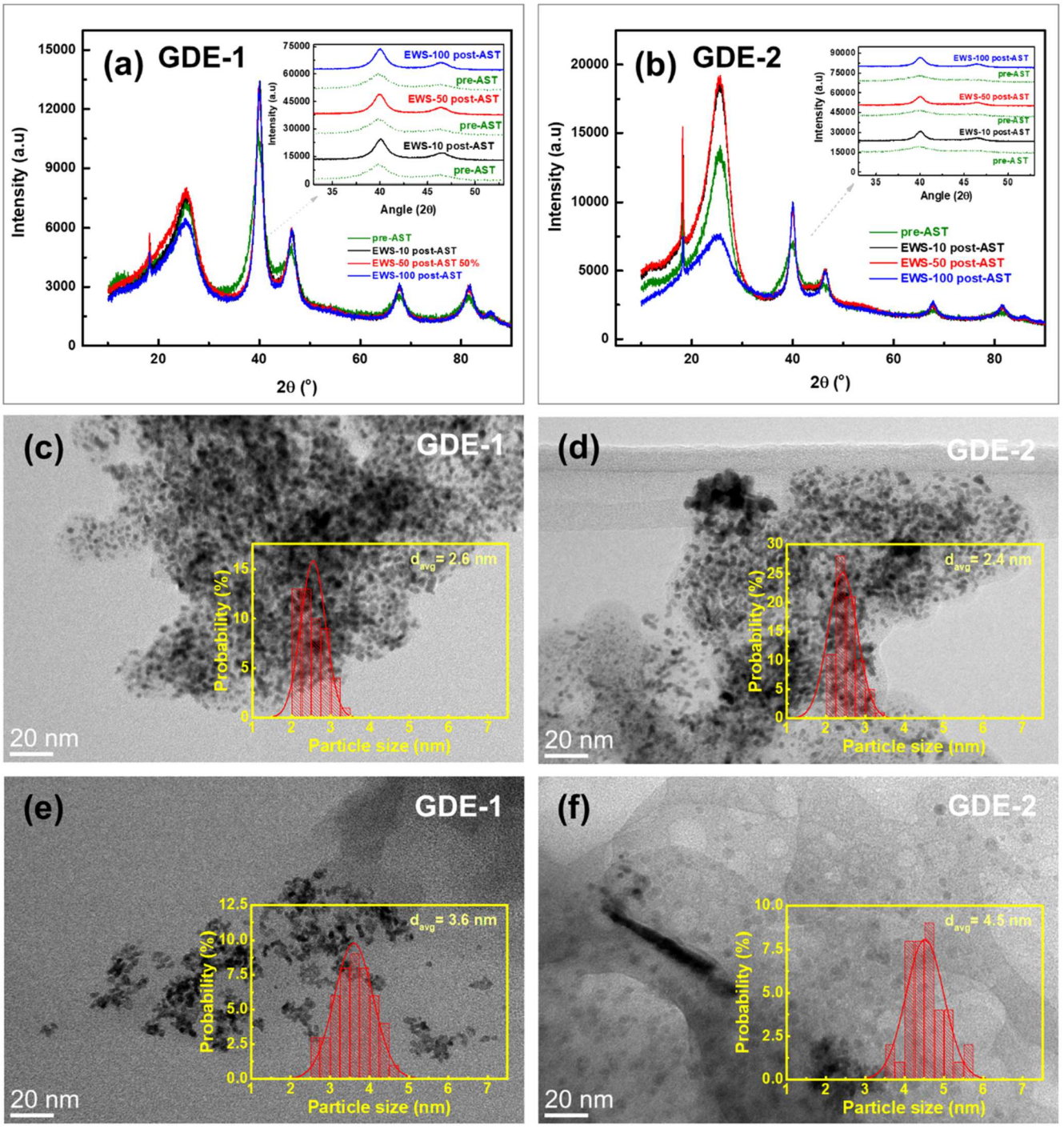

Figure 3. X-ray diffraction patterns of pre-AST and post-AST (a) GDE-1, and (b) GDE-2 electrode subjected to EWS wetting procedure before the AST (Inset: zoom-in into the Pt(111) and Pt(200) diffraction peaks). The solid and dashed lines correspond to the pre-AST (0 stress cycles) and post-AST (after 1600 stress cycles) XRD patterns, respectively. TEM images of the catalyst layers from the (c) resh GDE-1, (d) fresh GDE-2, (e) post-AST EWS-100 wetted GDE-1, and (f) post-AST EWS-100 wetted GDE-2 electrodes. Insets in the TEM images show the corresponding particle size distribution histograms for the Pt nanoparticles.

$$PSA\,(m^2 g_{Pt}^{-1}) = \frac{Total\ surface\ area\ of\ Pt\ crystallites \quad (m^2)}{Pt\ mass \quad (g)} \qquad \text{[E2]}$$

The detailed PSA calculation is explained in section 4.0 of SI. The PSA values give an estimate of the upper limit of the ECSA of the GDE ($ECSA_{\max} = PSA$). Moreover, utilization factor (U) — defined as the fraction of PSA of the electrocatalytically active entity (here Pt) accessible to the electrochemical reaction environment (and hence in reality contributing to the electrochemical activity) can be estimated as the ratio of measured ECSA to its maximum limit (Eq. E3).[44] Initial ECSA values were used in the U calculations.

$$U = \frac{ECSA\ (\mathrm{m^2 g^{-1}})}{PSA\ (\mathrm{m^2 g^{-1}})} \times 100 \qquad \text{[E3]}$$

The utilization factors of the electrodes subjected to EWS wetting using different ethanol fractions are summarized in Table III. The utilization factors for both the GDE−1 and GDE-2 electrodes increase with increasing ethanol fraction during EWS wetting. This

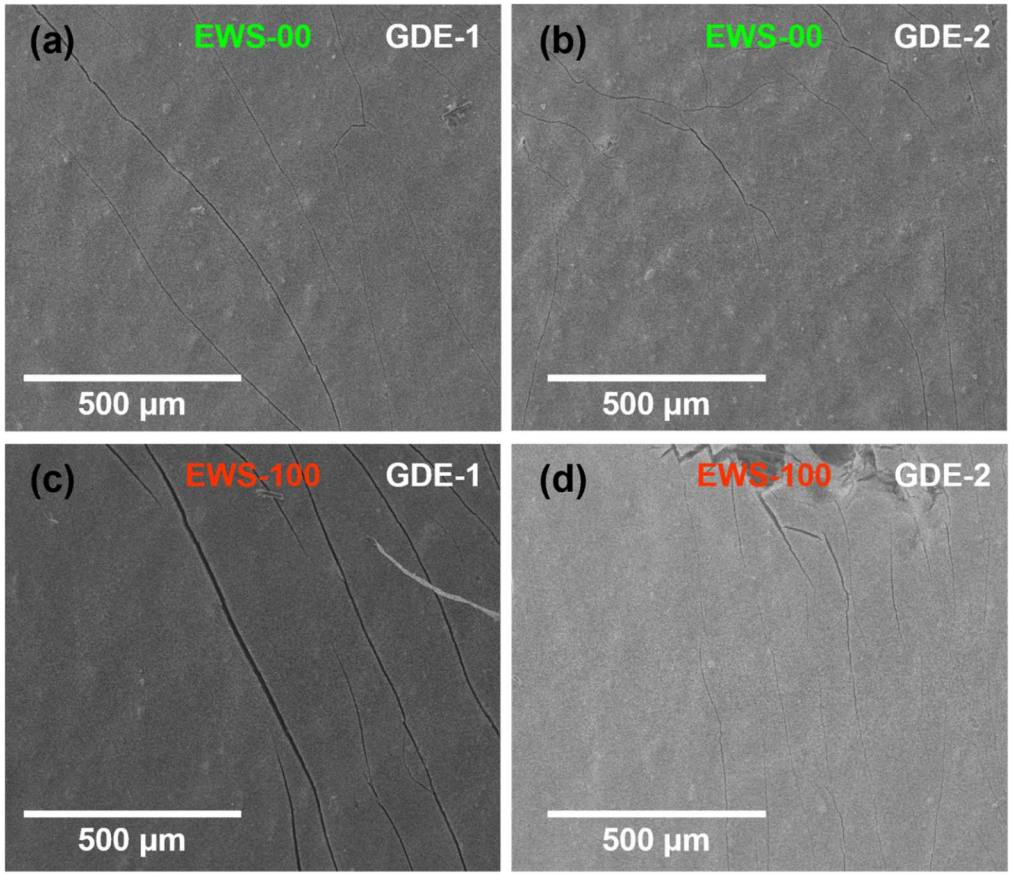

Figure 4. SEM images of the GDEs wetted using (a), (b) EWS-00 and (c), (d) EWS-100 solutions. (a) EWS-00 GDE-1, (b) EWS-00 GDE-2, (c) EWS-00 GDE-1, and (d) EWS-00 GDE-2.

Table III. Summary of parameters (initial ECSA, final ECSA, PSA, utilization factor, ECSA retention and Pt loading retention) obtained from the pre-AST and post-AST analysis of GDE-1 and GDE-2 electrodes wetted using EWS wetting.

Electrode	Ethanol fraction (% volume)	Initial ECSA (m^2/g)	Final ECSA (m^2/g)	PSA (m^2/g)	Utilization factor (%)	ECSA retention (%)	Pt loading retention (%)
GDE-1 electrode	10 (EWS-10)	86 ± 2	64 ± 1	107	80	74	95
	50 (EWS-50)	92 ± 1	66 ± 2	107	86	72	94
	100 (EWS-100)	98 ± 1	67 ± 1	107	92	68	91
GDE-2 electrode	10 (EWS-10)	87 ± 3	33 ± 2	124	70	38	77
	50 (EWS-50)	110 ± 1	59 ± 2	124	88	54	64
	100 (EWS-100)	110 ± 2	59 ± 1	124	88	54	76

trend in the utilization factor further indicates that the hydrophobicity of GDEs decreases when higher ethanol fraction (50% or 100%) is used to wet the electrodes, leading to better wettability and, ultimately, exposing more Pt sites to the electrolyte.

Interestingly, for both types of GDEs, the trend in utilization factor is the opposite of that in the ECSA/Pt retention with ethanol fraction. Again, Pt retention on the GDE during AST, calculated by measuring the areal Pt loadings on the GDE sample before (pre-AST) and after AST (post-AST), shown in Table III, suggests, in general, decreasing Pt retention (higher dissolution) with increasing the ethanol volume fraction used for the EWS wetting. These observations suggest that when more Pt sites are initially exposed to the electrolyte (by using a higher ethanol fraction), more sites are available for dissolution/redeposition and Ostwald ripening, leading to lower ECSA/Pt retention during the AST.

The difference in the extent of Pt crystallite growth and stability in GDE−1 and GDE-2 is most likely to stem from the difference in the Pt nanoparticle size, PTFE content, and Pt loading. The Pt particles in GDE-2 (∼3.5 nm) are smaller than those in GDE−1 (∼5.5 nm). It is well established in the literature that smaller Pt particles grow faster and are less stable during AST. In addition, GDE-2 has lower PTFE content than GDE-1, making it less hydrophobic. As a result, after wetting, more Pt particles in GDE-2 are exposed to the electrolyte, undergo dissolution and redeposition, leading to lower durability and higher crystallite growth.

Effect of EWS wetting on the GDE surface morphology.—As the EWS wetting, especially EWS-50 and EWS-100, improves the wettability of the HT-PEMFC GDEs significantly, it could be used to make the room-temperature electrochemical characterization possible. However, in LT-PEMFC GDEs containing Nafion ionomer in the CL, wetting in solutions with high ethanol content alters the CL structure through its partial detachment and/or redistribution. To investigate the effect of EWS wetting on the structural integrity of the HT-PEMFC GDEs, EWS- wetted GDEs were examined carefully through (i) visual inspection for physical detachment of the CL

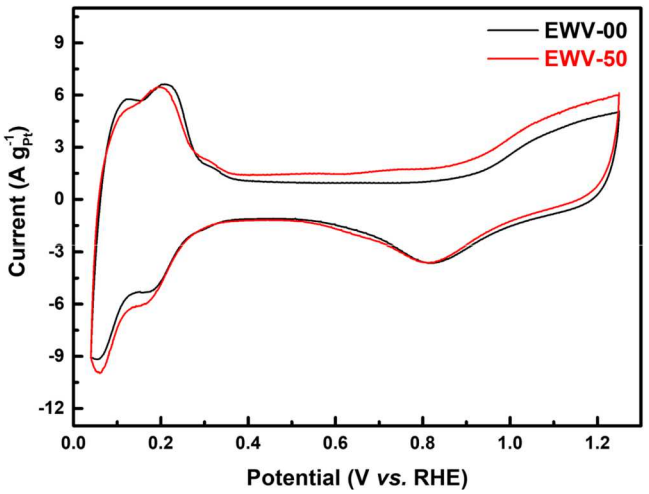

Figure 5. Cyclic voltammograms recorded in Ar-saturated 14.85 M H_3PO_4 at a scan rate of 0.01 V s^{-1} on the GDE-1 electrode samples subjected to the WEV-00 and WEV-50 wetting treatments.

during EWS wetting, (ii) XRF analysis of the EWS-wetted GDEs to observe any Pt loss, and (iii) SEM imaging to observe any changes in the CL morphology of the EWS- wetted GDE samples. Both visual inspection and XRF analysis rule out CL detachment/damage. The SEM images of the EWS-00 and EWS-100 GDE-1 and GDE-2 electrodes shown in Fig. 4 reveal similar surface morphologies of the corresponding EWS-00 and EWS-100 samples, confirming no structural changes due to EWS-100 wetting. A few cracks observed in all the GDE samples appear to originate from their manufacturing process, especially due to stresses developed during drying. This implies that the use of the EWS wetting process does not affect the physical structure/stability and morphology of the GDEs.

Ethanol-water vapor (EWV) wetting and its relevance to HT-PEMFC testing/operation.—As established in the previous section, EWS wetting improves the HT-PEMFC GDE wettability, making them suitable for room-temperature electrochemical characterizations in liquid electrolytes. Could such a wetting be used in the HT-PEMFC testing/operation to reduce the time required for initial activation (break-in) of the cell? To answer the question, the EWS wetting process was further explored. As it can only be performed on the GDEs and not on the assembled single or stack HT-PEMFC, EWV wetting, a modified form of the EWS wetting, by exposing the GDEs with the vapors of ethanol-water mixture, as described in Table I, was implemented here. The cyclic voltammograms recorded on the GDE 1 samples subjected to the wetting treatments EWV-00 and EWV-50 (Fig. 5) show observable differences in the H_{upd} region. The ECSA values of the EWV-00 and EWV-50 GDEs are 64 m^2g^{-1} and 71 m^2g^{-1}, respectively. This indicates that EWV wetting has effects on ESCA and utilization factor similar to those of the EWS wetting. Further, as compared to pure water wetting (EWS-00), the water vapor wetting (EWV-00) appears relatively effective, with the CV of the GDE-1 subjected to EWV-00 wetting shows characteristic features of Pt (Fig. 5), while that for the GDE-1 subjected to EWS-00 wetting appears featureless (Fig. 2a). This is possibly due to adsorption of the water vapor in the CL pores followed by condensation. However, from a practical point of view, for room- temperature GDE characterizations in liquid electrolyte cells, EWS wetting may be preferred over EWV wetting.

Further, we hypothesize that, since the EWV wetting procedure improves the GDE wettability and increases the utilization factor for the room-temperature liquid cell measurements, it might be applied to a single/stack HT-PEMFCs MEAs to improve wetting and hence achieve faster activation/reduced break-in time. As ethanol-water vapors can be introduced into the assembled HT-PEMFC MEA, for example, integrating the ethanol-water vapors with the reactant gases, EWV wetting could be practically used in such systems.

To test this hypothesis, the impact of EWV wetting on the cell break-in process was tested in a single HT-PEMFC. For this purpose, two different types of MEAs, constructed using GDEs based on carbon paper and carbon cloth GDLs, were tested using a standard break-in/activation protocol. The break-in/activation time for the MEA constructed with carbon paper GDL is ∼72 h, and during this

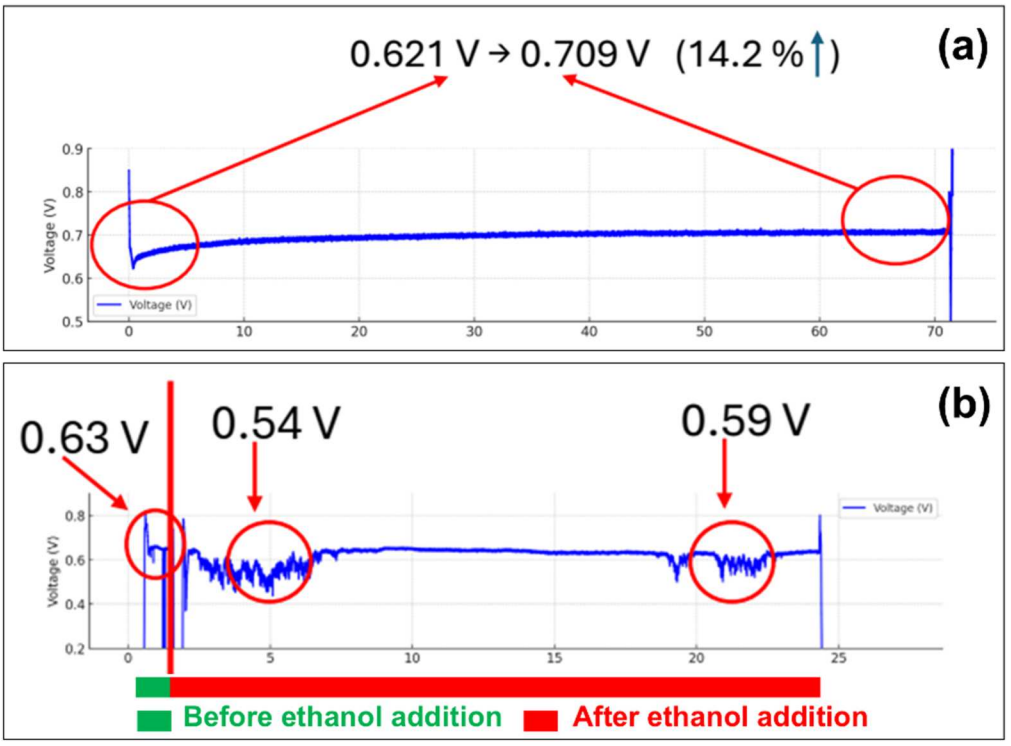

Figure 6. Variations of the cell voltage during single cell break-in procedure under (a) standard conditions and (b) in the presence of ethanol vapors.

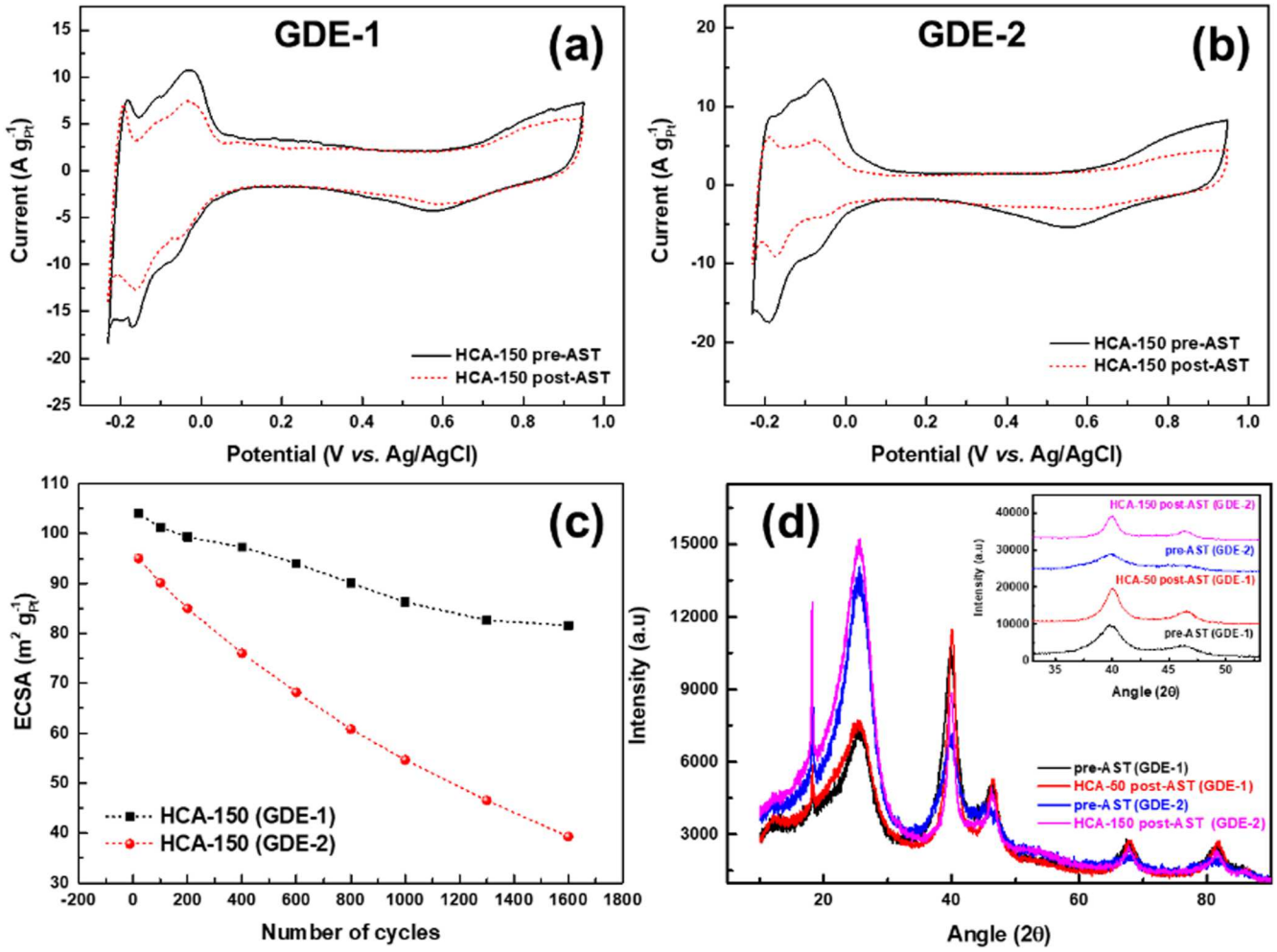

Figure 7. Cyclic voltammograms on HCA wetted (a) GDE-1 and (b) GDE-2 electrode recorded in argon-saturated 14.85 M H_3PO_4 at a scan rate of 0.01 V s^{-1}. The solid and dashed lines represent the pre-AST and post-AST voltammograms, respectively. (c) Variation of the ECSA in the GDE-1 electrode and (d) the GDE-2 electrode with the number of cycles performed during AST.

break-in/activation, the cell voltage increased from 0.621 V to a stable value of 0.709 V (14% increment) (Fig. S5a). On the other hand, the MEA constructed with carbon cloth as the GDL showed a cell voltage of ∼0.701 V from the beginning of the break-in process and remained stable throughout (Fig. S5b). This confirmed greater break-in requirements and challenges for the carbon paper-based HT-PEMFC MEAs. With the expectation of reducing the break-in time and attaining stable cell voltage faster, ethanol vapor treatment of the carbon paper GDL-based MEA was performed using the protocol shown in Fig. S2. Introduction of ethanol vapor during break-in reduced the cell voltage from 0.63 V (initial) to ∼0.59 V, with instability observed during break-in/activation (Fig. S6). A comparison of the break-in process of the single HT-PEMFC consisting of the carbon paper-based MEA without and with the ethanol vapor treatment is shown in Fig. 6. The slight decrease in cell voltage observed after the introduction of ethanol vapor into the cell may be due to changes in the interfacial structure of the MEA.

As an exploration of the reasoning why GDE wetting might not be an issue in the single cell/stack HT PEMFC MEAs, another wetting procedure, namely HCA wetting (Table I), was investigated for wetting the GDE-1 and GDE-2 electrodes by exposure (for 10 min) of the corresponding GDEs in the 14.85 M H_3PO_4 heated to 150 °C. SEM images of GDEs wetted at 150 °C reveal (Fig. S4) reveal no major cracks or openings in the CL, which indicates that HCA-150 wetting does not alter their morphology and structure.

The effect of HCA-150 wetting on the electrochemistry of the GDE-1 and GDE-2 samples can be confirmed by comparing the pre-AST cyclic voltammograms of Figs. 7a, 7b with the corresponding ones (EWS-00) in Fig. 2a, 2b. As expected, the H_{upd} charge (and hence the ECSA values) and oxide formation charge decreased significantly when the GDE-1 and GDE-2 electrodes were subjected to AST (Fig. 7c). For both electrodes, ECSA decreases with the number of AST cycles, and this trend depends on the wetting conditions. ECSA retention (from CV) and Pt retention from XRF analysis of post-AST electrodes show that a higher utilization factor led to lower ECSA/Pt retention.

The results of the AST assessment and other quantities are summarized in Table S1. Initial ECSA values of the GDEs subjected to the HCA-150 wetting are comparable to the corresponding values for the GDEs wetted as per the EWS-50 or EWS-100 wetting protocol. Again, the Pt crystallite size estimated from XRD analysis of pre-AST and post-AST electrodes (Fig. 7d, Table S2) shows that the average Pt crystallite size increases during the AST assessment in both GDE-1 and GDE-2 electrodes. These observations are similar to those for the GDEs subjected to the EWS-10/EWS-50 or EWS-100 wetting. This indicates that the HCA-150 wetting process has an effect similar to that of the EWS wetting on the HT-PEMFC GDEs. GDEs in the assembled HT-PEMFC MEAs soaked in the concentrated H_3PO_4 and MEAs were heated to 100 °C before and during the exposure to the ethanol vapors (Fig. S1), GDEs most probably were under a complete wet condition similar to that of the EWS-50/EWS-100 wetting. Hence, exposure to ethanol vapors did not change/improve the wetting in this case.

This shows that the EWS/EWV wetting protocols are highly useful for initial screening of GDEs for HT-PEMFCs, where

electrochemical performance and stability assessment through room temperature studies in liquid electrolyte cells are performed. However, realizing these benefits in a single-cell configuration will require additional effort, including integrating wetting treatments into ink formulation and processing, adjusting electrode assembly fabrication procedures, and optimizing the acid-doping step. Because break-in procedures vary widely, no single method is universally optimal. The appropriate choice depends on factors such as membrane type, ionomer and catalyst composition, catalyst loading, and membrane thickness.[46] Methods such as ex situ water soaking condition the membrane to reduce ng interfacial resistance, whereas voltage cycling is more effective for catalyst activation.[34] Some approaches also suit specific membranes or electrode materials. Therefore, selecting a PEMFC break-in method requires evaluating the membrane, catalyst, and ionomer characteristics and understanding the strengths and limitations of each technique.[47,48]

Conclusions

Effects of the pre-wetting of HT-PEMFC GDEs on the catalyst utilization and durability under potentiodynamic AST were investigated in a liquid cell three-electrode configuration. Pre-wetting of the GDEs either in (1) water or an ethanol-water solution (0%, 10%, 50% and 100% ethanol) at room temperature, (2) ethanol-water vapor, and (3) concentrated orthophosphoric acid (14.85 M) heated to 150 °C were explored. Electrochemical studies conducted at room temperature in the orthophosphoric acid (14.85 M) electrolyte suggest that all three pre-wetting methods significantly affect the catalyst utilization and durability of the GDEs. Although the use of higher ethanol fraction (50% or 100%) in ethanol-water solution wetting resulted in better initial catalyst utilization, it has an adverse effect on the durability of the catalyst when subjected to AST assessment, which ultimately led to lower ECSA/Pt retention. Similar trends in catalyst utilization and ECSA/Pt retention were observed when the electrodes were wetted in H_3PO_4 heated to 150 °C. Use of a higher ethanol fraction or high-temperature wetting exposed more Pt sites initially for dissolution/ redeposition and Ostwald ripening. Both ethanol wetting and high-temperature wetting have similar effect on catalyst utilization and Pt retention. The implementation of the ethanol pre-wetting in a single-cell indicated that although the pre-wetting protocol is highly useful for initial screening of HT-PEMFC GDE performance and stability in the three-electrode test, it still requires additional consideration/optimization to translate these benefits into a single cell.

Acknowledgments

Authors acknowledge the financial support from Innovation Fund Denmark, Grand Solutions, Nr. 2105–00024B, project ReHTPEM; Slovenian Research Agency (research core funding No. P2–0089) and CENN Nanocenter for the use of the Transmission Electron Microscope Jeol JEM-2100.

ORCID

Rajan Maurya https://orcid.org/0000-0002-7580-4535
Per Morgen https://orcid.org/0000-0001-6994-9597
Saso Gyergyek https://orcid.org/0000-0002-7325-2984
Vahid Karimi https://orcid.org/0000-0002-9011-0339
Mengfan Zhou https://orcid.org/0000-0002-7980-2959
Na Li https://orcid.org/0000-0002-1267-6185
Fan Zhou https://orcid.org/0000-0002-3673-2903
Vincenzo Liso https://orcid.org/0000-0002-7597-3849
Raghunandan Sharma https://orcid.org/0000-0001-5962-983X
Shuang Ma Andersen https://orcid.org/0000-0003-1474-0395

References

1. H. Gasteiger and S. Yan, *J. Power Sources*, **127**, 162 (2004).
2. T. Schmidt, H. Gasteiger, G. Stäb, P. Urban, D. Kolb, and R. Behm, *J. Electrochem. Soc.*, **145**, 2354 (1998).
3. H. A. Gasteiger, S. S. Kocha, B. Sompalli, and F. T. Wagner, *Appl. Catalysis B*, **56**, 9 (2005).
4. A. J. Bard, L. R. Faulkner, and H. S. White, *Electrochemical Methods: Fundamentals and Applications* (Wiley) (2022).
5. T. Okada, S. Møller-Holst, O. Gorseth, and S. Kjelstrup, *J. Electroanal. Chem.*, **442**, 137 (1998).
6. H. Ito, T. Maeda, A. Nakano, and H. Takenaka, *Int. J. Hydrogen Energy*, **36**, 10527 (2011).
7. C. M. Zalitis, D. Kramer, and A. R. Kucernak, *Phys. Chem. Chem. Phys.*, **15**, 4329 (2013).
8. P. J. Petzoldt, J. T. H. Kwan, A. Bonakdarpour, and D. P. Wilkinson, *J. Electrochem. Soc.*, **168**, 026507 (2021).
9. S. Martens, L. Asen, G. Ercolano, F. Dionigi, C. Zalitis, A. Hawkins, A. M. Bonastre, L. Seidl, A. C. Knoll, and J. Sharman, *J. Power Sources*, **392**, 274 (2018).
10. R. Sharma and S. M. Andersen, *ACS Catal.*, **8**, 3424 (2018).
11. S. Bose, T. Kuila, T. X. H. Nguyen, N. H. Kim, K.-t Lau, and J. H. Lee, *Prog. Polym. Sci.*, **36**, 813 (2011).
12. Z. Fu, L. Lu, C. Zhang, Q. Xu, X. Zhang, Z. Gao, and J. Li, *Sustainable Energy Technologies and Assessments*, **57**, 103181 (2023).
13. S. Lee, S. Mukerjee, E. A. Ticianelli, and J. McBreen, *Electrochim. Acta*, **44**, 3283 (1999).
14. C. Yang, P. Costamagna, S. Srinivasan, J. Benziger, and A. B. Bocarsly, *J. Power Sources*, **103** (2001).
15. R. Rosli, A. Sulong, W. Daud, M. Zulkifley, T. Husaini, M. Rosli, E. Majlan, and M. Haque, *Int. J. Hydrogen Energy*, **42**, 9293 (2017).
16. Q. Li, R. He, J. O. Jensen, and N. J. Bjerrum, *Chem. Mater.*, **15**, 4896 (2003).
17. S. Wang, X. Hu, Z. Zhou, Q. Wang, K. Ye, S. Sui, M. Hu, and F. Jiang, *Sustainable Energy Technologies and Assessments*, **60**, 103529 (2023).
18. G. S. Avcioglu, B. Ficicilar, and I. Eroglu, *Int. J. Hydrogen Energy*, **43**, 18632 (2018).
19. W. J. Lee, J. S. Lee, H.-Y. Park, H. S. Park, S. Y. Lee, K. H. Song, and H.-J. Kim, *Int. J. Hydrogen Energy*, **45**, 32825 (2020).
20. X. Zhang, Y. Pan, L. Cai, Y. Zhao, and J. Chen, *Energy Convers. Manage.*, **144**, 217 (2017).
21. F.-B. Weng, C.-Y. Hsu, and C.-W. Li, *Int. J. Hydrogen Energy*, **35**, 3664 (2010).
22. A. M. C. Luna, G. A. Camara, V. A. Paganin, E. A. Ticianelli, and E. R. Gonzalez, *Electrochem. Commun.*, **2**, 222 (2000).
23. C. W. Bezerra, L. Zhang, H. Liu, K. Lee, A. L. Marques, E. P. Marques, H. Wang, and J. Zhang, *J. Power Sources*, **173**, 891 (2007).
24. S. Thomas, S. S. Araya, J. R. Vang, and S. K. Kær, *Int. J. Hydrogen Energy*, **43**, 14691 (2018).
25. F. Van Der Linden, E. Pahon, S. Morando, and D. Bouquain, *J. Power Sources*, **575**, 233168 (2023).
26. Z. Qi and A. Kaufman, *J. Power Sources*, **109**, 227 (2002).
27. S. S. Kocha and B. G. Pollet, *Current Opinion in Electrochemistry*, **31**, 100843 (2022).
28. T. Van Nguyen, M. V. Nguyen, K. J. Nordheden, and W. He, *J. Electrochem. Soc.*, **154**, A1073 (2007).
29. R. Pinkhas, *Preconditioning of gas diffusion layers for improved performance and operational stability of PEM fuel cells*, US patent, US8415076 (2015), https://patents.google.com/patent/US8415076B2/en?oq=US8415076.
30. G. Tsotridis, A. Pilenga, G. De Marco, and T. Malkow, *EU harmonised test protocols for PEMFC MEA testing in single cell configuration for automotive applications JRC Science for Policy repor, EUR 27632 EN* (2015), https://publications.jrc.ec.europa.eu/repository/handle/JRC99115.
31. Z. Qi and A. Kaufman, *J. Power Sources*, **114**, 21 (2003).
32. Z. Qi and A. Kaufman, *J. Power Sources*, **111**, 181 (2002).
33. M. Zhiani, I. Mohammadi, and S. Majidi, *Int. J. Hydrogen Energy*, **42**, 4490 (2017).
34. J. hee Song, M. soo Kim, Y. rim Kang, and D. kyu Kim, *Journal of Energy Storage*, **44**, 103338 (2021).
35. F. A. de Bruijn, V. Dam, and G. Janssen, *Fuel cells*, **8**, 3 (2008).
36. S. S. Araya, I. F. Grigoras, F. Zhou, S. J. Andreasen, and S. K. Kær, *Int. J. Hydrogen Energy*, **39**, 18343 (2014).
37. Y. Wang, C.-Y. Wang, and K. Chen, *Electrochim. Acta*, **52**, 3965 (2007).
38. R. Sharma and S. M. Andersen, *ACS Appl. Mater. Interfaces*, **10**, 38125 (2018).
39. J. C. Jiménez-García, D. F. R. Flores, R. H. Acosta, M. I. Velasco, E. A. Franceschini, and M. M. Mariscal, *Int. J. Hydrogen Energy*, **52**, 65 (2024).
40. Q. Meyer, S. Liu, K. Ching, Y. Da Wang, and C. Zhao, *J. Power Sources*, **557**, 232539 (2023).
41. D. V. Dao, G. Adilbish, T. D. Le, I.-H. Lee, and Y.-T. Yu, *RSC Adv.*, **9**, 15635 (2019).
42. Y. Hu, Z. Xia, C. Yang, J. Huang, S. Wang, and G. Sun, *Journal of Energy Chemistry*, **103**, 850 (2025).
43. S. Trasatti and O. Petrii, *Pure Appl. Chem.*, **63**, 711 (1991).
44. K. J. Omann, R. Sharma, P. Morgen, S. Gyergyek, M. J. Larsen, and S. M. Andersen, *ACS Appl. Energy Mater.*, **6**, 1294 (2023).
45. B. D. Cullity and R. Smoluchowski, *Phys. Today*, **10**, 50 (1957).
46. Y. Yurko and L. Elbaz, *Electrochim. Acta*, **389**, 138676 (2021).
47. R. N. Harilal, P. C. Ghosh, and T. Jana, *ACS Applied Polymer Materials*, **2**, 3161 (2020).
48. T. Tingelöf and J. K. Ihonen, *Int. J. Hydrogen Energy*, **34**, 6452 (2009).